

Cosmic-ray diffusion in collisionless plasmas including pressure anisotropy

M. S. Nakwacki*

Instituto de Astronomía y Física del Espacio (IAFE-CONICET), Ciudad Universitaria, Buenos Aires 1428, Argentina

J. Peralta-Ramos

Departamento de Física, Facultad de Ciencias Exactas y Naturales, Universidad de Buenos Aires and IFIBA-CONICET, Ciudad Universitaria, Buenos Aires 1428, Argentina

arXiv:1312.7822v1 [astro-ph.HE] 30 Dec 2013

Abstract

Using a hybrid kinetic magnetohydrodynamic formalism incorporating the effects of pressure anisotropy, we simulate the evolution of a turbulent collisionless plasma in six different models covering the sub/super-sonic and sub/super-Alfvénic regimes. Based on the power spectrum of the simulated magnetic field, we compute the particle diffusion coefficients for protons with kinetic energy in the 50 – 500 MeV range, and compare them to those obtained within standard magnetohydrodynamics. Our results show that the differences in the statistical properties of the magnetic field, generated by pressure anisotropy and its associated kinetic instabilities, have an appreciable impact on the diffusion coefficients of energetic protons. Moreover, the values of the diffusion coefficients that we obtain within each of the six models considered vary significantly.

Keywords: cosmic rays; diffusion; collisionless space plasma; pressure anisotropy

1. Introduction

A complete understanding of the transport of charged energetic particles through a magnetized turbulent plasma poses a challenge in many areas, ranging from fusion research to space physics. The main difficulty arises due to the stochastic nature of the magnetic field. In particular, the diffusion of charged particles in a fluctuating magnetic field has attracted a lot of attention due to its relation with cosmic ray transport. Different approaches have been developed to study particle diffusion in turbulent plasmas, among which the most well-known are the quasilinear theory (QLT) (Jokipii, 1966; Shalchi, 2005; Dosch et al., 2013; Schlickeiser & Vainio, 1998), hard-sphere scattering models (Gleeson, 1969), nonlinear guiding center formalisms (Matthaeus et al., 2003; Shalchi & Dosch, 2008), approaches based on velocity correlation functions (Bieber & Matthaeus, 1997), and test-particle simulations (Giacalone & Jokipii, 1999; Gao et al., 2011; Xu & Yan, 2013; Tautz et al., 2013; Tautz, 2013; Casse et al., 2002; Guo et al., 2010). For reviews on energetic particle transport through space plasmas see e.g. Jokipii (1971); Giacalone (1998, 2010); Parker (1965); Zweibel (2013); Jokipii (2008, 2010); Schlickeiser (1994); Potgieter (2013); Bruno & Carbone (2013) and references therein.

The diffusion of charged particles in a turbulent plasma is directly related to the statistical properties of the magnetic field. In weakly collisional plasmas, particles can exhibit anisotropic distributions with respect to the local magnetic field direction, that can survive for considerably long periods compared to dynamical timescales of certain systems. The interplay between temperature anisotropy, the kinetic instabilities that are triggered by it, and strong turbulence leads to complex phenomena in weakly collisional space plasmas that can affect their macroscopic evolution in nontrivial ways (Lazarian et al., 2012; Brandenburg & Lazarian, 2013; Matthaeus et al., 1995; Matteini et al., 2007; Maruca et al., 2011; Bale et al., 2009; Chen et al., 2010; Samsonov et al., 2007; Osman et al., 2013; Matteini et al., 2006; Osman et al., 2012; Servidio et al., 2013; Hellinger & Trávníček, 2008; Schekochihin et al., 2010; Kunz, 2011).

Collisionless plasmas are often described by the Maxwell-Vlasov equation, which is computationally quite demanding to solve. Fortunately, many properties of weakly collisional plasmas can be reasonably well described by fluid-like models, provided that some additional constraints are considered. The simplest fluid-like approximation is the well-known double adiabatic MHD model developed by Chew, Goldberg and Low (CGL) (Chew et al., 1956). A modified CGL-MHD model incorporating the anisotropy constraints due to kinetic instabilities has been used for modeling the solar wind and magnetosphere in numerical simulations (Samsonov et al., 2001, 2007; Meng et al.,

*Corresponding author

Email addresses: sole@iafe.uba.ar (M. S. Nakwacki),
jperalta@df.uba.ar (J. Peralta-Ramos)

2012b,a; Dzhilov et al., 2008). Similar models have been used in Kunz (2011) to study the heating of central regions of cold-core clusters of galaxies, in Sharma (2007) to investigate the magnetorotational instability in accretion disks around black holes, and in Santos-Lima et al. (2011) to simulate a turbulent dynamo. In Kowal et al. (2011), it was shown that the presence of the instabilities driven by temperature anisotropy has strong impact on the evolution of the plasma density, velocity and magnetic field. More recently, CGL-MHD numerical simulations were performed (Nakwacki et al., 2012; Santos-Lima et al., 2013) to study fast growing magnetic fluctuations in the smallest scales which operate in the collisionless plasma that fills the intra-cluster medium. A comparison of Faraday Rotation Maps obtained from CGL-MHD and MHD simulations was carried out in Ref. Nakwacki et al. (2013).

It turns out that the statistical properties of the turbulent magnetic field obtained from the CGL-MHD formalism are in general quite different from those obtained from MHD (except in the high plasma β plasma case, see Santos-Lima et al. (2013)). These differences are largely due to the effect of kinetic instabilities such as the firehose and mirror instabilities, both of them triggered by the pressure anisotropy present in collisionless plasmas. It is therefore of interest to quantify the impact of differences in the statistical properties of the magnetic field (that result from the presence of pressure anisotropy) on the transport of energetic particles through a magnetized fluctuating plasma.

In this paper, we perform CGL-MHD and MHD 3D numerical simulations of the turbulent magnetic field, using different plasma parameters that cover the sub/super-Alfvénic and the sub/supersonic regimes. Using the simulated magnetic field, we calculate the diffusion coefficients for protons with kinetic energies in the 50–500 MeV range. Since our aim here is to determine the impact of pressure anisotropy on the diffusion coefficients for particle propagation through a magnetized plasma in the simplest possible setting, we shall stick to the QLT. We must point out that in recent years the QLT has been shown to present several limitations (see, e.g., Dosch et al. (2009); Giacalone (2010); Bieber & Matthaeus (1997); Tautz et al. (2013); Tautz (2013)). The use of more elaborate and accurate formalisms to model particle transport in turbulent plasmas is left for future work.

We should note that, to the best of our knowledge, the comparison of diffusion coefficients computed from CGL-MHD and MHD simulations has not been attempted before. In Ref. de Gouveia Dal Pino et al. (2011), the CGL-MHD model was used to study particle acceleration in the intergalactic medium, which is nearly collisionless, taking into account kinetic effects that affect the turbulent magnetic field distribution by making it much more wrinkled than in a standard MHD turbulent system, and therefore substantially affecting cosmic-ray propagation.

The paper is organized as follows. In Section 2 we briefly outline the QLT derivation of the diffusion coefficients

for energetic particles in a fluctuating magnetic field, and also provide details of the numerical scheme used to simulate the evolution of the anisotropic plasma. In Section 3 we present and discuss our results, and in Section 4 we give our conclusions and outlook.

2. Theoretical setup

2.1. Diffusion coefficients in quasilinear theory

The diffusion coefficients D_{\parallel} and D_{\perp} are computed from the first-order QLT for axisymmetric turbulence originally derived from the Fokker-Planck equation by Jokipii (1966, 1971). The validity of the QLT is discussed in detail in Jokipii (1966, 1971) (see also Shalchi (2005); Giacalone (1998)), but for clarity we will enumerate the assumptions made in its derivation. First, the fluctuating magnetic field is such that $\langle(\delta B)^2\rangle/\langle B_0^2\rangle \ll 1$, where B_0 and δB are the mean magnetic field and a typical fluctuation of the magnetic field, respectively. This implies that particle motion can be well described by the two-point correlation of the magnetic field. Second, the changes in pitch angle of the particles due to scattering with magnetic irregularities are assumed to be small with respect to the correlation length of the magnetic field, and thus the pitch angle distribution can be taken as isotropic. And lastly, the variation of the particle distribution function n along the direction of the particle’s path is small over the distance in which a particle is scattered appreciably in pitch angle. The latter requirement implies that the time variation of n is due to diffusion motion, which is much slower than individual particle motion.

For completeness, we shall briefly state the main results of the QLT that we will use throughout. We assume that there is a mean field $B_0(\vec{r})\hat{z}$, and consider random fluctuations $\vec{B}_1(\vec{r}) = B_{1x}\hat{x} + B_{1y}\hat{y} + B_{1z}\hat{z}$, so that $\vec{B}(\vec{r}) = B_0(\vec{r})\hat{z} + \vec{B}_1(\vec{r})$. Define $\omega = \frac{Ze}{\gamma m_0 c}\vec{B}$, where Ze and m_0 are the particle’s charge and rest mass, c is the speed of light, and $\gamma = (1 - V^2/c^2)^{-1/2}$ with V the particle’s speed. The basic quantity is the two-point correlation function

$$R_{ij}(\eta, \psi, \zeta) = \langle \omega_{1i}(x, y, z) \omega_{1j}(x + \eta, y + \psi, z + \zeta) \rangle \quad (1)$$

In what follows, we will compute the diffusion coefficients along given trajectories, which for simplicity take to be parallel to the \hat{z} axis. This corresponds in an approximate way to the situation we are interested in, namely one in which a spacecraft measuring the magnetic field travels through the plasma along these trajectories. To this end, we will need the one-dimensional power spectrum, which can be calculated in the plasma rest frame as follows (assuming the spacecraft travels at a constant speed V_w in the \hat{z} direction)

$$P_{ij}(f) = \frac{\gamma^2 m_0^2 c^2}{Z^2 e^2} \int_{-\infty}^{\infty} R_{ij}(0, 0, \zeta) e^{-2\pi i f \zeta / V_w} \frac{d\zeta}{V_w} \quad (2)$$

The diffusion coefficients are then given by Jokipii (1971).

$$D_{\perp} = \frac{1}{2} \int_0^1 \frac{\langle (\Delta x)^2 \rangle}{\Delta t} d\mu \quad (3)$$

and

$$D_{\parallel} = \frac{2V^2}{9} \left[\int_0^1 \frac{\langle (\Delta \mu)^2 \rangle}{\Delta t} \right]^{-1} \quad (4)$$

where

$$\frac{\langle (\Delta \mu)^2 \rangle}{\Delta t} = \frac{Z^2 e^2}{\gamma^2 m_0^2 c^2} \frac{(1 - \mu^2) V_w}{|\mu| V} P_{XX}(f^*) \quad (5)$$

and

$$\frac{\langle (\Delta x)^2 \rangle}{\Delta t} = \frac{Z^2 e^2}{\gamma^2 m_0^2 c^2} \frac{|\mu| V V_w}{2\omega_0^2} \left[2P_{XX}(0) + \frac{1 - \mu^2}{\mu^2} P_{ZZ}(f^*) \right] \quad (6)$$

In these expressions, $\mu = V_z/V$ is the cosine of the particle's pitch angle and

$$f^* = \frac{V_w \omega_0}{2\pi \mu V} \quad (7)$$

is the resonant frequency.

2.2. Numerical simulations of the turbulent magnetic field

To simulate the dynamics of the collisionless magnetized plasma in the presence of pressure anisotropy, we use an MHD formalism with a Chew-Golberger-Low double-isothermal closure (Chew et al., 1956), as implemented in the numerical code developed in Kowal et al. (2011).

The equations for the magnetic field \vec{B} , particle velocity \vec{V} and density ρ can be written as

$$\frac{\partial \rho}{\partial t} + \vec{\nabla} \cdot (\rho \vec{V}) = 0 \quad (8)$$

$$\frac{\partial \vec{B}}{\partial t} - \vec{\nabla} \times (\vec{V} \times \vec{B}) = 0 \quad (9)$$

and

$$\frac{\partial(\rho \vec{V})}{\partial t} + \vec{\nabla} \cdot \left[\left(a_{\perp}^2 \rho + \frac{B^2}{8\pi} \right) \mathcal{I} - (1 - \alpha) \vec{B} \vec{B} \right] = \vec{f} \quad (10)$$

The term \vec{f} is a random solenoidal large-scale driving force representing the turbulence driving, which is driven at wave scale $k = 2.5$ (i.e. 2.5 times smaller than the size of the box used in the simulations). $P = p_{\perp} \mathcal{I} + (p_{\parallel} - p_{\perp}) \hat{b} \hat{b}$ is the pressure tensor with components $p_{\parallel} = a_{\parallel}^2 \rho$ and $p_{\perp} = a_{\perp}^2 \rho$ parallel and perpendicular to the magnetic field direction $\hat{b} = \vec{B}/|\vec{B}|$ (\mathcal{I} stands for the unit matrix). a_{\parallel}

and a_{\perp} are constants and represent speed of sounds along the parallel and perpendicular directions to the magnetic field. The quantity α is defined as $\alpha = (p_{\parallel} - p_{\perp})/(2P_{\text{mag}})$, where $P_{\text{mag}} = B^2/(8\pi)$ is the magnetic pressure.

We do not take into account viscosity and diffusion in the equations. The numerical integration of the system evolution governed by the CGL-MHD equations were performed by using the second-order shock-capturing Godunov-scheme code and the time integration was done with the second-order Runge-Kutta method. Further details about the CGL-MHD code used here can be found in Kowal et al. (2011) (see also Santos-Lima et al. (2011, 2013); Nakwacki et al. (2012)).

In order to study the dependence of the diffusion coefficients on the structure of the magnetic field, we have performed simulations for six different initial conditions covering the sub/super-Alfvénic and the sub/supersonic regimes, as indicated in Table 1. The models can be further divided into strong or weak turbulence regimes, corresponding to $\rho \delta v^2 > p_{\parallel} \delta B^2$ and $\rho \delta v^2 < p_{\parallel} \delta B^2$, respectively, where δv and δB are root mean square values of velocity and magnetic field intensity. In all of the cases studied, the initial density is set equal to 5 cm^{-3} , while the initial particle velocity is zero. In all of our numerical simulations we use a box of 0.1 AU and a mesh-grid of 256^3 points. The magnetic field is a sum of a mean field and fluctuations, i.e. $\vec{B} = \vec{B}_0 + \delta \vec{B}$. Initially, $\delta \vec{B} = 0$. The mean magnetic field is set in the \hat{z} direction, $\vec{B}_0 = B_0 \hat{z}$. The anisotropy parameter α is taken to be time-independent. We note that the values of the squared sound speed c_s^2 corresponding to each model is the same in the MHD and the CGL-MHD simulations.

Table 1: Initial conditions and some features of the six models studied. The initial magnitude of the magnetic field B_0 is given in nT. supS/subS stand for supersonic/subsonic, while supA/subA stand for super-Alfvénic/sub-Alfvénic.

Model	B_0	a_{\parallel}	a_{\perp}	Regime	Instability
1	5.0	1.0	2.0	subS-subA	Mirror
2	5.0	1.0	0.5	subS-subA	Firehose
3	0.5	0.1	0.2	supS-supA	Mirror
4	0.5	0.1	0.05	supS-supA	Firehose
5	0.5	1.0	0.5	subS-supA	Firehose
6	5.0	0.1	0.2	supS-subA	Mirror

Models 1 and 2 correspond to weak turbulence in the subsonic and sub-Alfvénic regime. The difference between these two cases is that in model 1 mirror instabilities are triggered by pressure anisotropy, while in model 2 firehose instabilities are triggered. Models 3 and 4 correspond to strong turbulence in the supersonic and super-Alfvénic regimes, and differ with each other in the kind of kinetic instability that is present. Mirror and firehose instabilities arise in models 3 and 4, respectively. We note that models 3 and 4 correspond to the conditions prevailing in the solar wind. Finally, model 5 corresponds to the subsonic and super-Alfvénic regime and presents firehose instabili-

ties in weak turbulence, while model 6 corresponds to the supersonic and sub-Alfvénic regime and presents mirror instabilities in strong turbulence.

To compute the diffusion coefficients, we use the magnetic field at a time corresponding to a fully developed turbulent cascade. We have averaged out the values of D_{\parallel} and D_{\perp} obtained from the 36 trajectories closest to the center of the $x - y$ plane and parallel to the \hat{z} axis. We have checked that reasonable convergence in these values is achieved provided that more than ~ 16 trajectories are considered in the average. For all of the models studied here, the standard deviation obtained for this set of 36 trajectories is less than a tenth of the value of the diffusion coefficients, which sets our resolution for D_{\parallel} and D_{\perp} .

3. Results and discussion

3.1. Magnetic field

In this section we shall briefly discuss the main differences between the plasma configuration attained at large times in the six models described in Table 1. We recall that at this stage of the evolution of the plasma, the turbulent cascade is fully developed. We shall focus on the features of the magnetic field in each regime, since this is the physical quantity that is most directly connected to the diffusion coefficients, but to provide a more complete overview we will also comment on the particle’s velocity and density distributions. Detailed discussions about the statistical properties of the magnetic field, the velocity and the density for these models in MHD and CGL-MHD can be found in Kowal et al. (2011).

Figures 1 and 2 depict the magnetic field intensity in the center of the computational domain for models 1, 2, and 3, and for models 4, 5, 6, respectively. The CGL-MHD results are shown in the left column, while the standard MHD case is shown in the right column.

In the case of weak turbulence in the subsonic and sub-Alfvénic regime (first row of Figure 1), corresponding to model 1, the presence of mirror instabilities produces changes in the velocity distribution, accelerating the plasma along the magnetic field lines resulting in the increase of the effective sonic Mach number and more elongated structures. As the turbulence is weak, the instabilities can grow without being suppressed by the turbulent motions of the gas. This results in large differences between the magnetic field structure obtained in CGL-MHD and in MHD.

The subsonic, sub-Alfvénic weak turbulence regime corresponding to model 2 is shown in the second row of Figure 1. This case presents strong firehose instabilities responsible for deformation of the magnetic field lines. The curved magnetic lines tend to slow down and trap the flowing gas. Since the growth rate is larger at small scales, we expect this effect to create more granulated maps. As in model 1, the instabilities can freely grow without being suppressed by the turbulent motions of the gas. Here, the firehose

instability is responsible for the generation of small-scale magnetic field fluctuations that tangle the field lines and result in an increase of the perpendicular pressure, thus leading to the isotropization of the fluctuations with respect to the magnetic field lines. Comparing the MHD and CGL-MHD cases, it is seen that in the former the magnetic field intensity is more elongated.

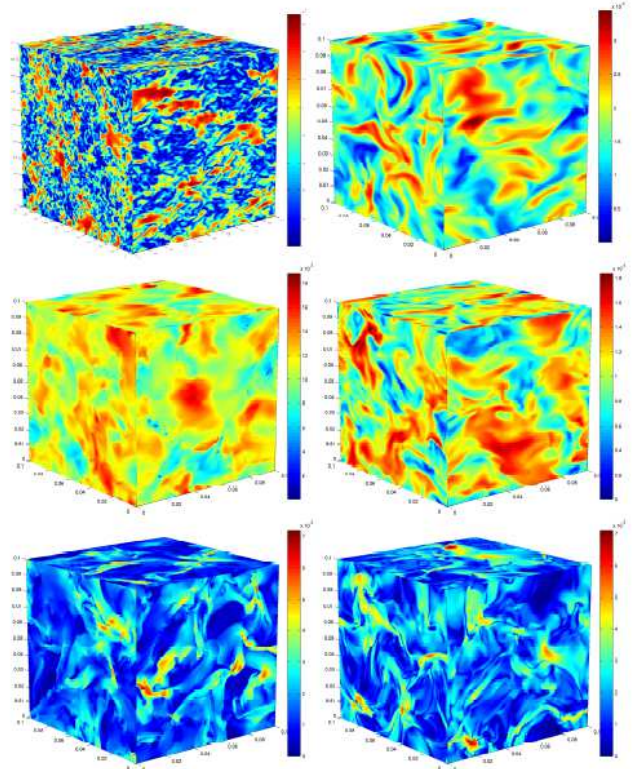


Figure 1: Central slices of computational domain of the magnetic field intensity (CGL-MHD left and MHD right) for models 1, 2, and 3.

In the case of model 3 (supersonic and super-Alfvénic), shown in the third row of Figure 1, the granulated structures are not present. The strong turbulence is able to destroy the magnetic field’s configuration attained by the mirror instabilities.

As in the previous case, model 4, corresponding to the supersonic and super-Alfvénic regime with firehose instabilities, does not present granulated structure, as shown in the first row of Figure 2. Instead, the magnetic field intensity presents a more homogeneous structure. Note that the structure of the magnetic field obtained in CGL-MHD for models 3 and 4 is very similar to the one obtained in MHD. However, slight differences are visible in the case of model 4, with the magnetic field corresponding to CGL-MHD being more homogeneous than the MHD one.

Model 5, corresponding to the subsonic and super-Alfvénic weak turbulence regime, is shown in the second row of Figure 2. The strong firehose instabilities triggered in this regime deform the magnetic field lines as in model 2, producing a very granulated distribution of the magnetic field

intensity that is very different from the structure found in MHD.

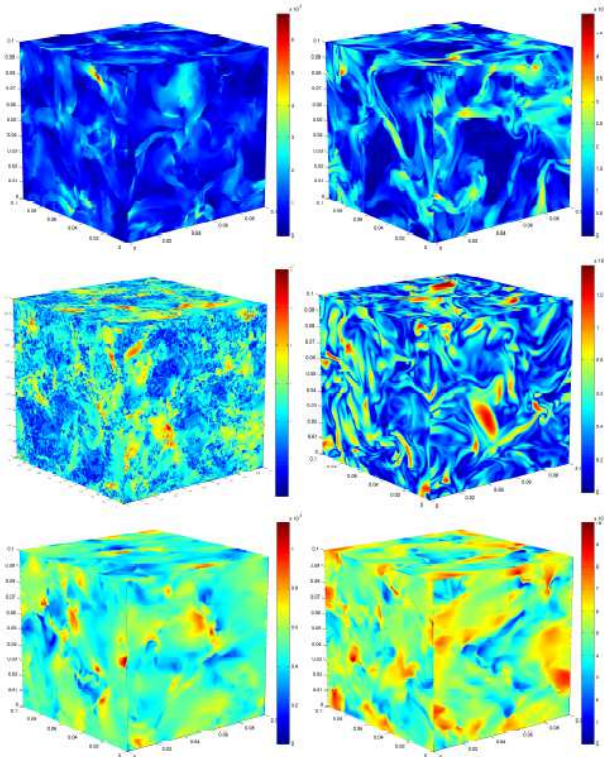


Figure 2: Central slices of computational domain of the magnetic field intensity (CGL-MHD left and MHD right) for models 4, 5, and 6.

The third row of Figure 2 shows the results obtained in model 6, corresponding to the supersonic and sub-Alfvénic strong turbulence regime. In this case, the evolution of turbulence causes a mirror instability in most of the computational domain. The instability, although it is somewhat suppressed by strong turbulent motion, is responsible here for slowing the gas and reducing the effective sonic Mach number. Note, however, that the differences between the structure of the magnetic field intensity in MHD and CGL-MHD are not large, being the CGL-MHD case slightly more homogeneous than its MHD counterpart.

As it can be seen from Figures 1 and 2, the late-time configuration of the magnetic field intensity is appreciably different not only among the different models, but also between MHD and CGL-MHD within each model. In particular, the differences in the magnetic field structure obtained in both formalisms is most significant in models 1, 2 and 5. This is a direct consequence of the fact that in these models the turbulence is weak, so the evolution of the instabilities is not strongly affected by turbulent motions. Moreover, as shown in Ref. Kowal et al. (2011), since these models are also subsonic the density and velocity spectra computed from CGL-MHD simulations show enhanced power at small scales as compared to the ones obtained in MHD.

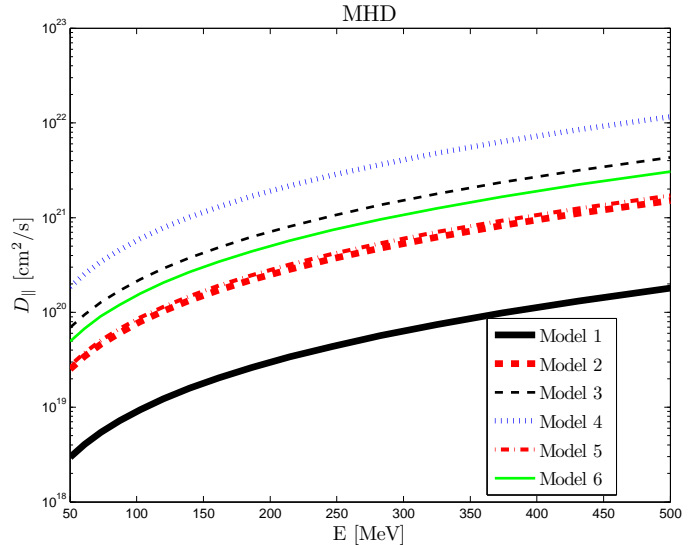


Figure 3: D_{\parallel} as a function of proton energy, as obtained from MHD numerical simulations for the six models considered.

In the next section, we shall relate the features discussed above to the values of the diffusion coefficients corresponding to a particle transversing the plasma.

3.2. Diffusion coefficients

We start by comparing the diffusion coefficients obtained in the different models considered, in MHD and in CGL-MHD. Figures 3 and 5 show D_{\parallel} and D_{\perp} as a function of proton energy, as obtained from MHD simulations. Figures 4 and 6 show the same quantities but corresponding to CGL-MHD simulations.

The first thing to notice from Figures 3-6 is that the values of D_{\parallel} and D_{\perp} are appreciably sensitive to the plasma parameters that determine the turbulent regime. The differences between the values of D_{\parallel} and D_{\perp} corresponding to the six models considered can be as large as three orders of magnitude. This shows that the diffusion coefficients computed from first-order QLT depend significantly on the turbulent regime in which the collisionless plasma evolves.

It is worth noting also that the dependence of the diffusion coefficients on energy is practically independent of the plasma regime. This result is in line with that of Ref. Shalchi et al. (2009), where it was shown that a non-Gaussian magnetic field distribution only affects the amplitude of diffusion coefficients. From Figures 3-6, it is seen that D_{\parallel} increases with increasing energy, while D_{\perp} is weakly dependent on energy. The values that we obtain for D_{\parallel} and D_{\perp} are of the order of those reported in previous observational and numerical studies (see, e.g., Giacalone (1998, 2010)), but we emphasize that it is not our purpose here to make detailed comparisons to other cosmic-ray transport models.

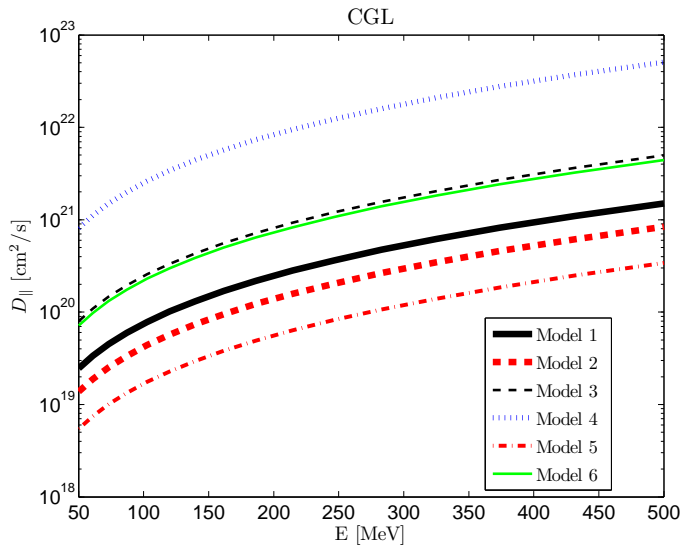


Figure 4: D_{\parallel} as a function of proton energy, as obtained from CGL-MHD numerical simulations for the six models considered.

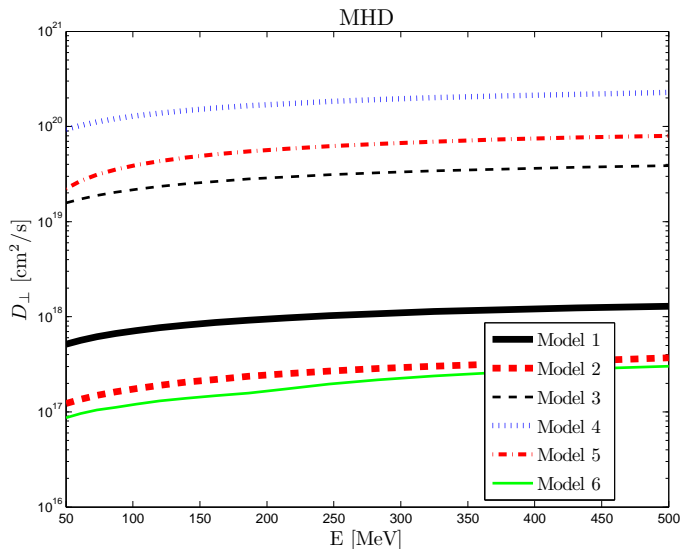


Figure 5: D_{\perp} as a function of proton energy, as obtained from MHD numerical simulations for the six models considered.

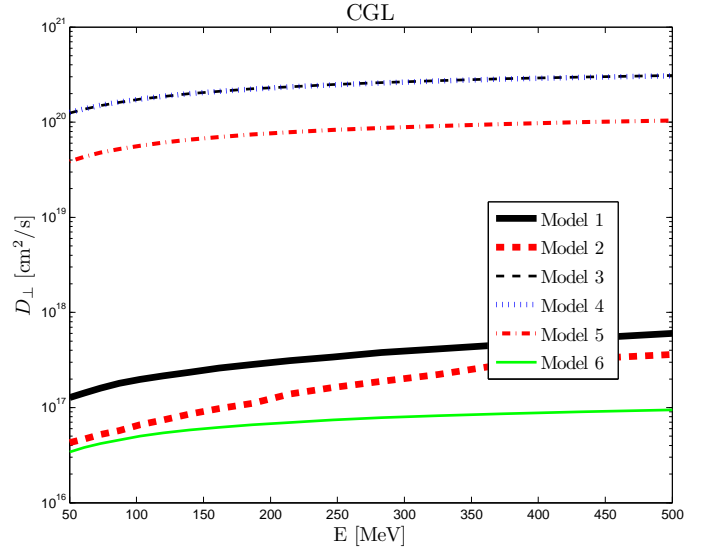


Figure 6: D_{\perp} as a function of proton energy, as obtained from CGL-MHD numerical simulations for the six models considered.

As it can be seen from Figure 3, in MHD the parallel diffusion is largest in model 4, corresponding to the supersonic and super-Alfvénic strong turbulence regime, and least important in model 1, corresponding to the subsonic and sub-Alfvénic weak turbulence regime. In CGL-MHD (Figure 4), parallel diffusion is again larger in model 4, but smallest in model 5 instead, that corresponds to the subsonic and super-Alfvénic weak turbulence regime with firehose instabilities. The latter feature may be due to the fact that in model 5, firehose instabilities can grow freely and tend to produce more granulated structures along the direction of the mean magnetic field, so that the parallel diffusion suffered by a particle moving parallel to the mean magnetic field is, on average, reduced.

For D_{\perp} in MHD (shown in Figure 5), the largest values are obtained once again in model 4, while the smallest ones are obtained in model 6, corresponding to the supersonic and sub-Alfvénic strong turbulence regime. In CGL-MHD (Figure 6), perpendicular diffusion is most important in model 3 (supersonic and super-Alfvénic strong turbulence regime) and model 4, being the values in these two models very close to each other. The smallest values of D_{\perp} are again obtained in model 6. The fact that D_{\perp} is smallest for model 6 both in MHD and CGL-MHD can be explained by noting that in this model the local magnetic field grows as turbulence develops, resulting in strong magnetic breaking. In contrast to what happens in model 5, in model 6 the magnetic field is strong so that the perpendicular flows are not capable of destroying the magnetic configuration generated by strong turbulence. We stress that this behavior is not related to kinetic instabilities, but rather to the strong turbulence regime.

We shall now focus on the differences between the results obtained from MHD and from CGL-MHD. From Fig-

ures 3 and 4, it is seen that the values of D_{\parallel} corresponding to models 1 and 4 in CGL-MHD are enhanced by an order of magnitude as compared to MHD. In contrast, the values corresponding to models 2 and 5 in CGL-MHD are somewhat suppressed, probably due to the effect of firehose instabilities which in these two models can grow freely and generate small-scale fluctuations of the magnetic field along the direction of the mean magnetic field. The values of D_{\parallel} corresponding to models 3 and 6 do not change much when going from MHD to CGL-MHD.

Going over to D_{\perp} , we see from Figures 5 and 6 that the values of D_{\perp} corresponding to models 1, 2 and 6 are somewhat suppressed in CGL-MHD as compared to MHD. In contrast, the value of D_{\perp} corresponding to model 3 is enhanced by one order of magnitude in CGL-MHD as compared to MHD. It is seen also that the values of D_{\perp} corresponding to models 4 and 5 are roughly the same in both formalisms.

Some insight into the effect of pressure anisotropy on the diffusion coefficients can be achieved by comparing the ratio of perpendicular to parallel diffusion coefficients, D_{\perp}/D_{\parallel} , that is obtained in the two formalisms. Figures 7-12 show D_{\perp}/D_{\parallel} as a function of proton energy, as obtained from each of the six models for MHD and CGL-MHD.

It is seen that the ratio decreases with increasing particle's energy. D_{\perp}/D_{\parallel} typically decreases by approximately one order of magnitude in the energy range considered.

For models 1, 4 and 6, shown in Figures 7, 10 and 12 the ratio in MHD larger than the one in CGL-MHD. Note that in models 1 and 4 the ratio in MHD is larger than 10^{-2} , while in model 6 the ratio is smaller than $\sim 10^{-3}$. In contrast, for models 3 and 5 (Figures 9 and 11) the ratio in CGL-MHD is larger than the one in MHD. In model 5, the ratio in CGL-MHD is close to $\sim 10^1$ at the lowest energies considered, while the ratio in MHD is roughly the same as in model 4. For model 3, the ratio reaches $\sim 10^0$ in CGL-MHD and $\sim 10^{-1}$ in MHD.

For model 2, shown in Figure 8, the ratios corresponding to MHD and CGL-MHD are very similar to each other and rather small $\sim 10^{-3} - 10^{-2}$, and become almost indistinguishable to the accuracy of our calculations. The similarity of the values of D_{\perp}/D_{\parallel} in MHD and CGL-MHD that we obtain in model 2 is due to the effect of the firehose instabilities on the magnetic field fluctuations. Model 2 corresponds to a weak turbulence regime in which these instabilities can grow freely, and whose main effect is to isotropize the magnetic field fluctuations. The isotropization of the magnetic field fluctuations is not evident in models 4 and 5, which also involve firehose instabilities. In model 4 this is because the turbulence is strong enough to destroy the configuration attained by the effect of the firehose instabilities. In model 5, the magnetic field is weak (whereas in model 2 it is strong), and therefore the motion perpendicular to the local magnetic field lines is able to destroy the magnetic field configuration generated by the firehose instabilities.

The largest difference in the values of the ratio obtained

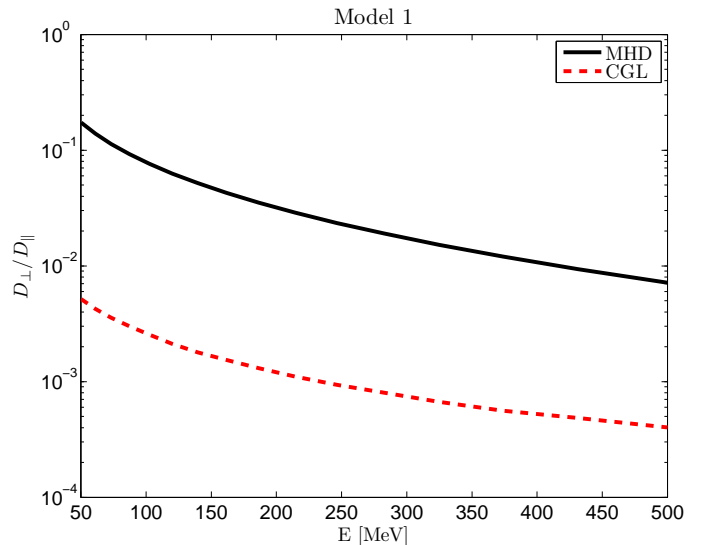


Figure 7: D_{\perp}/D_{\parallel} as a function of proton energy, as obtained from model 1 in MHD and CGL-MHD.

in MHD and CGL-MHD is obtained in model 1, where it can reach almost two orders of magnitude. We recall that this model corresponds to a weak turbulence regime with mirror instabilities. These kinetic instabilities tend to increase the anisotropy of magnetic field fluctuations, thus leading to a larger difference between MHD and CGL-MHD. Model 3 also presents mirror instabilities, but the model corresponds to a strong turbulence regime, so that the effect of mirror instabilities is largely washed out by the turbulent motion of the plasma.

4. Conclusions

Within the first-order quasi-linear theory of particle propagation through a fluctuating magnetized plasma, we have computed the parallel and perpendicular diffusion coefficients for low energy protons travelling through a collisionless plasma. The turbulent magnetic field evolution was modeled using a hybrid kinetic-magnetohydrodynamics formalism that incorporates the effect of pressure anisotropy and its associated instabilities, or otherwise by standard magnetohydrodynamics. We have analysed six plasma models with parameters corresponding to the sub/supersonic and sub/super-Alfvénic regimes, leading to weak turbulence dominated by mirror or firehose instabilities, or else strong turbulence in which the magnetic configuration generated by instabilities is largely washed out.

Our main result is that the diffusion coefficients calculated using magnetic fields obtained from MHD-like numerical simulations that include or not pressure anisotropy can differ substantially. Moreover, we have shown that the values of the diffusion coefficients depend significantly on the regime in which the collisionless plasma evolves. These results prompts us to perform detailed studies of energetic

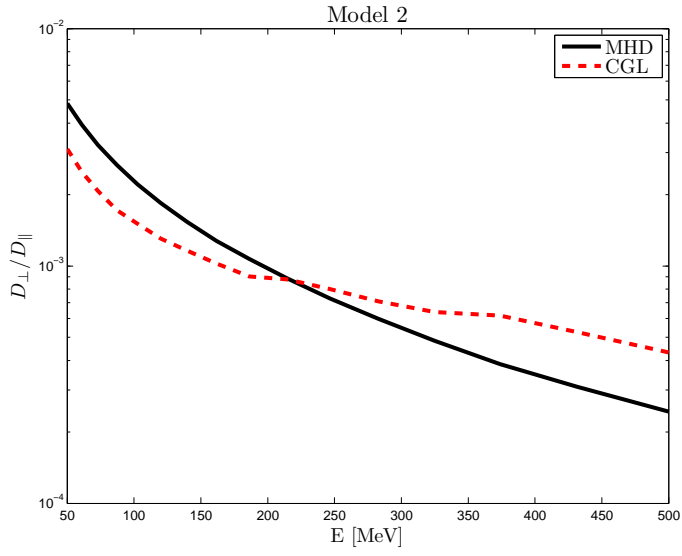


Figure 8: D_{\perp}/D_{\parallel} as a function of proton energy, as obtained from model 2 in MHD and CGL-MHD.

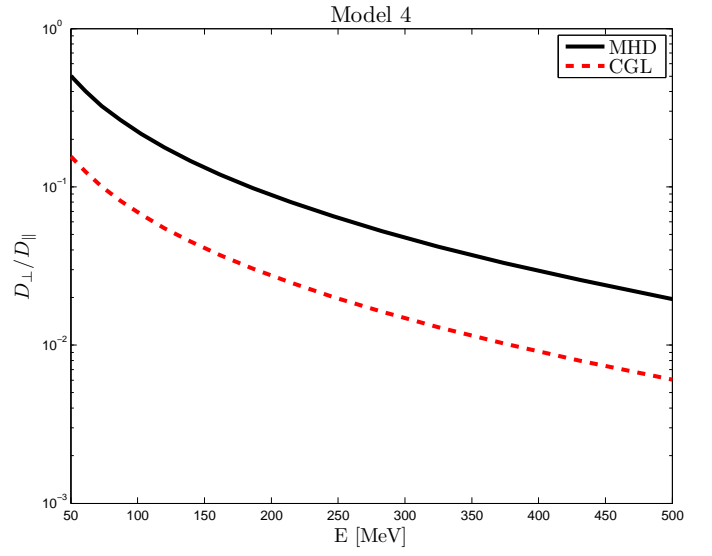


Figure 10: D_{\perp}/D_{\parallel} as a function of proton energy, as obtained from model 4 in MHD and CGL-MHD.

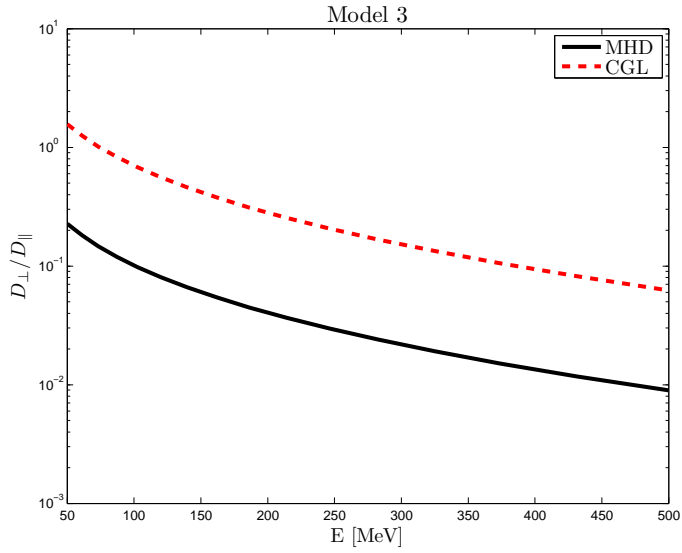


Figure 9: D_{\perp}/D_{\parallel} as a function of proton energy, as obtained from model 3 in MHD and CGL-MHD.

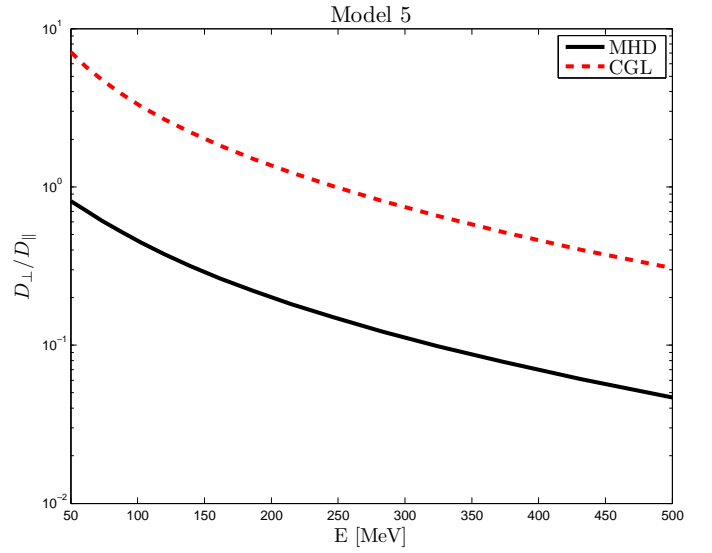


Figure 11: D_{\perp}/D_{\parallel} as a function of proton energy, as obtained from model 5 in MHD and CGL-MHD.

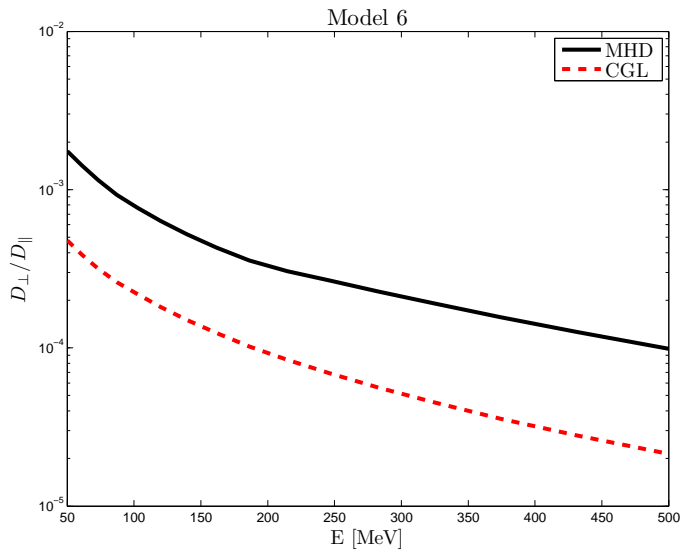


Figure 12: D_{\perp}/D_{\parallel} as a function of proton energy, as obtained from model 6 in MHD and CGL-MHD.

particle propagation through collisionless turbulent space plasmas where pressure anisotropy is present, using for this purpose more accurate formalisms that remove the limitations of the first-order quasi-linear theory used here. Work is in progress in this direction.

We thank G. Kowal for making the numerical code *Godunov* available to us. This work has been supported in part by the Consejo Nacional de Investigaciones Científicas y Técnicas (CONICET) of Argentina.

References

Bale, S. D., Kasper, J. C., Howes, G. G., et al. 2009, *Physical Review Letters*, 103, 211101

Bieber, J. W. & Matthaeus, W. H. 1997, *The Astrophysical Journal*, 485, 655

Brandenburg, A. & Lazarian, A. 2013, *Space Sci. Rev.*, 178, 163

Bruno, R. & Carbone, V. 2013, *Living Reviews in Solar Physics*, 10, 2

Casse, F., Lemoine, M., & Pelletier, G. 2002, *Phys. Rev. D*, 65, 023002

Chen, C. H. K., Horbury, T. S., Schekochihin, A. A., et al. 2010, *Physical Review Letters*, 104, 255002

Chew, G. F., Goldberger, M. L., & Low, F. E. 1956, *Royal Society of London Proceedings Series A*, 236, 112

de Gouveia Dal Pino, E. M., Kowal, G., Lazarian, A., & Santos-Lima, R. 2011, *ArXiv e-prints*

Dosch, A., Shalchi, A., & Weinhorst, B. 2009, *Advances in Space Research*, 44, 1326

Dosch, A., Shalchi, A., & Zank, G. P. 2013, *Advances in Space Research*, 52, 936

Dzhalilov, N. S., Kuznetsov, V. D., & Staude, J. 2008, *Astron. Astrophys.*, 489, 769

Gao, X., Lu, Q., & Wang, S. 2011, *Astrophys. Space Sci.*, 335, 399

Giacalone, J. 1998, *Space Sci. Rev.*, 83, 351

Giacalone, J. 2010, *Energetic particle transport*, ed. C. J. Schrijver & G. L. Siscoe (Cambridge University Press), 233

Giacalone, J. & Jokipii, J. R. 1999, *The Astrophysical Journal*, 520, 204

Gleeson, L. J. 1969, *Planet. Space Sci.*, 17, 31

Guo, F., Jokipii, J. R., & Kota, J. 2010, *The Astrophysical Journal*, 725, 128

Hellinger, P. & Trávníček, P. M. 2008, *Journal of Geophysical Research (Space Physics)*, 113, 10109

Jokipii, J. R. 1966, *The Astrophysical Journal*, 146, 480

Jokipii, J. R. 1971, *Reviews of Geophysics and Space Physics*, 9, 27

Jokipii, J. R. 2008, *Journal of Atmospheric and Solar-Terrestrial Physics*, 70, 442

Jokipii, J. R. 2010, *AGU Fall Meeting Abstracts*, D3

Kowal, G., Falceta-Gonçalves, D. A., & Lazarian, A. 2011, *New Journal of Physics*, 13, 053001

Kunz, M. W. 2011, *MNRAS*, 417, 602

Lazarian, A., Vlahos, L., Kowal, G., et al. 2012, *Space Sci. Rev.*, 173, 557

Maruca, B. A., Kasper, J. C., & Bale, S. D. 2011, *Physical Review Letters*, 107, 201101

Matteini, L., Landi, S., Hellinger, P., et al. 2007, *Geophys. Res. Lett.*, 34, 20105

Matteini, L., Landi, S., Hellinger, P., & Velli, M. 2006, *Journal of Geophysical Research (Space Physics)*, 111, 10101

Matthaeus, W. H., Bieber, J. W., & Zank, G. P. 1995, *Reviews of Geophysics*, 33, 609

Matthaeus, W. H., Qin, G., Bieber, J. W., & Zank, G. P. 2003, *The Astrophysical Journal Letters*, 590, L53

Meng, X., Tóth, G., & Gombosi, T. I. 2012a, in *Astronomical Society of the Pacific Conference Series*, Vol. 459, *Numerical Modeling of Space Plasma Slows (ASTRONUM 2011)*, ed. N. V. Pogorelov, J. A. Font, E. Audit, & G. P. Zank, 340

Meng, X., Tóth, G., Liemohn, M. W., Gombosi, T. I., & Runov, A. 2012b, *Journal of Geophysical Research (Space Physics)*, 117, 8216

Nakwacki, M. S., de Gouveia Dal Pino, E. M., Kowal, G., & Santos-Lima, R. 2012, *Journal of Physics Conference Series*, 370, 012043

Nakwacki, M. S., de Gouveia Dal Pino, E. M., Kowal, G., Santos-Lima, R., & Falceta-Gonçalves, D. A. 2013, in preparation

Osman, K. T., Matthaeus, W. H., Hnat, B., & Chapman, S. C. 2012, *Physical Review Letters*, 108, 261103

Osman, K. T., Matthaeus, W. H., Kiyani, K. H., Hnat, B., & Chapman, S. C. 2013, *Physical Review Letters*, 111, 201101

Parker, E. N. 1965, *Planet. Space Sci.*, 13, 9

Potgieter, M. 2013, *Living Reviews in Solar Physics*, 10, 3

Samsonov, A. A., Alexandrova, O., Lacombe, C., Maksimovic, M., & Gary, S. P. 2007, *Annales Geophysicae*, 25, 1157

Samsonov, A. A., Pudovkin, M. I., Gary, S. P., & Hubert, D. 2001, *Journal of Geophys. Res.*, 106, 21689

Santos-Lima, R., de Gouveia Dal Pino, E. M., Kowal, G., et al. 2013, *ArXiv e-prints*

Santos-Lima, R., de Gouveia Dal Pino, E. M., Lazarian, A., Kowal, G., & Falceta-Gonçalves, D. 2011, in *IAU Symposium*, Vol. 274, *IAU Symposium*, ed. A. Bonanno, E. de Gouveia Dal Pino, & A. G. Kosovichev, 482–484

Schekochihin, A. A., Cowley, S. C., Rincon, F., & Rosin, M. S. 2010, *MNRAS*, 405, 291

Schlickeiser, R. 1994, *Astrophys J. Sup.*, 90, 929

Schlickeiser, R. & Vainio, R. 1998, *Astrophys. Space Sci.*, 264, 457

Servidio, S., Osman, K. T., Valentini, F., et al. 2013, *ArXiv e-prints*

Shalchi, A. 2005, *Physics of Plasmas*, 12, 052905

Shalchi, A. & Dosch, A. 2008, *The Astrophysical Journal*, 685, 971

Shalchi, A., le Roux, J. A., Webb, G. M., & Zank, G. P. 2009, *Journal of Physics A Mathematical General*, 42, H5501

Sharma, P. 2007, *PhD thesis*, PhD Thesis, 2007

Tautz, R. C. 2013, *Astron. Astrophys.*, 558, A148

Tautz, R. C., Dosch, A., Effenberger, F., Fichtner, H., & Kopp, A. 2013, *Astron. Astrophys.*, 558, A147

Xu, S. & Yan, H. 2013, *The Astrophysical Journal*, 779, 140

Zweibel, E. G. 2013, *Physics of Plasmas*, 20, 055501